INFLUENCE OF STARCH CONTENT ON THE PROPERTIES OF LOW-COST MICROFILTRATION CERAMIC MEMBRANES

M-M. Lorente-Ayza [a] *, E. Sánchez [a], V. Sanz [a], S. Mestre [a]

[a] Instituto Universitario de Tecnología Cerámica. Universitat Jaume I. Castellón (Spain).

***Corresponding Author**: M-Magdalena Lorente-Ayza

Phone: +34 964 34 24 24

Fax: +34 964 34 24 25

E-mail: magda.lorente@itc.uji.es

Postal address: *Instituto de Tecnología Cerámica*

Campus Universitario Riu Sec

Av. Vicent Sos Baynat s/n

12006 Castellón (Spain)

Abstract

The use of starch as pore former is frequent in the fabrication of porous ceramic membranes, since starches are cheap, innocuous and environmentally friendly. A study has been conducted to evaluate the influence of potato starch content (0-30 wt %) and sintering temperature (1100 and 1400ºC) on low-cost ceramic microfiltration membranes. The raw materials were a mixture of kaolin, alumina and starch, from which membrane specimens were shaped by uniaxial dry pressing.

The results indicated that the percentage of potato starch did affect the properties of the membrane. Thus, an increase of starch content provoked a reduction of bulk density (an increase of porosity) a rise of water permeability and a substantial modification (coarsening) of the pore size distribution. This effect deals with the role as pore former of starch, which burns out when fired. More interestingly, it was experimentally observed that the effect of starch was particularly effective for starch percentages higher than 10 wt% once a connected coarse pore network is developed. On the other hand, an increase in

sintering temperature from 1100 to 1400ºC also influenced membranes' characteristics but the effect was much less significant than that of starch content.

A percolation analysis based on the Effective Medium Approximation (EMA) contact model allowed to conclude that the critical porosity calculated corresponds to a starch content of 10.2 wt%, which agrees quite well with the estimation from experimental results. Finally, tortuosity was calculated with a simple model derived from Hagen-Poiseuille equation. The obtained data showed that tortuosity factor decreased as the starch content or sintering temperature increased. These findings are consistent with SEM analysis and pore size determination.

***Keywords**: A. Precursors: organic; B. Porosity; B. Microstructure-final; E. Membranes.*

1. Introduction

The interest in low-cost ceramic membranes has recently increased since they combine high performance (as high thermal and mechanical stability, long life and good chemical stability) with economy (compared with habitual ceramic membranes available in market, made of alumina, zirconia or titania) [1,2]. The properties of the ceramic membranes are mainly determined by their composition, the pore-former content and the sintering temperature. The proposed compositions of low-cost ceramic membranes are very wide, depending on the nature of their raw materials: local clays [3–10] and kaolin [11–13], sepiolite [14], apatite [15,16], perlite [17,18], phosphate [19,20] or a mixture of some of them [21–26], among others.

To reach the optimum permeability level, most of the ceramic membranes' compositions include starch as pore former, in a proportion between 2 and 20 wt% [3,5,8–11,16–19,22,27]. Starch generates pores during its burning out around 500ºC; moreover, it is environmentally friendly, easy to burn out and very cheap [28]. The addition of starch granules to a mixture of inorganic raw materials yields ceramic membranes of greater porosity, tailored pore size and higher permeability. By adjusting the amount of starch added, a ceramic membrane of a specified pore size distribution and permeability can be obtained across a broad range. As reported examples, the mean pore sizes for alumina membranes ranged from 1 to

2 μm and apparent porosities increased from 23 to 44% as the added amount of starch rose from 0 wt% to 15 wt% [9], whereas in ball clay membranes the apparent porosity increased from 9 to 32% as the added amount of starch augmented from 0 wt% to 35 wt% (no data about pore sizes were published) [10].

Changes in maximum temperature of thermal cycle modify the properties of the ceramic membranes through its affect over sintering. The variations are reflected in porosity, which usually decreases when temperature increases, and pore size distribution, which shifts towards coarser pore sizes. Some studies about those phenomena have been previously reported. Membranes derived from ball clays showed a reduction in apparent porosity from 19 to 16 % when sintering temperature increased from 1000 to 1300°C [29]. Other membranes whose composition was based on a mixture of inexpensive raw materials (kaolin, quartz and different carbonates) displayed a similar trend: the porosity decreased from 40% to 22% when the sintering temperature increased from 900 to 1000ºC whereas the average pore size coarsened from 2.6 to 5.5 μm [30]. Similar trend have been found in ceramic membranes developed from a mixture of kaolin, pyrophyllite, feldspar, ball clay, quartz, and calcium carbonate: the porosity initially grew and then decreased in the range of 41–46 % and the average pore diameter augmented from 0.87 to 1.10 μm with an increment of sintering temperature from 850 to 1000ºC [31].

Water permeability is the most used parameter to characterise a ceramic membrane. Viscous flow of a Newtonian fluid through a porous medium can be described by Darcy's law, which relates the specific permeability to water (K_p, m^2) with the slope of the straight line obtained graphing the volume flux versus the pressure gradient (Eq. 1):

$$K_p = \frac{b \cdot \eta \cdot e}{S_0} \quad \text{[Eq. 1]}$$

where η is the water viscosity, e the membrane's thickness, b the value of the slope and S_0 the specific surface [32]. In addition, the best-known equation for describing the specific permeability of a medium (K_p, m^2) in terms of its structural properties is the Kozeny-Carman equation (Eq. 2):

$$K_p = \frac{1}{K_0 S_0^2} \frac{\varepsilon^3}{(1-\varepsilon)^2} \quad \text{[Eq. 2]}$$

where K_0 is the Kozeny constant, S_0 the specific surface, and ε the porosity of the membrane [33]. Assuming that the product $[K_0 \cdot S_0^2]$ varies little in a set of microfiltration membranes obtained with a similar process, the model predicts an approximately linear relationship between K_p and the porosity term $[\varepsilon^3/(1-\varepsilon)^2]$. The permeability coefficient (K_p) can also be related with the pore diameter (d) though the Hagen-Poiseuille equation:

$$K_p = \frac{\varepsilon_{sf} d^2}{32\eta\tau} \quad \text{[Eq. 3]}$$

being the water viscosity (η), the surface porosity (ε_{sf}) and the tortuosity factor (τ).
Assuming that the tortuosity can keep constant in a set of microfiltration membranes, the model prognosticates an approximately linear relationship between K_p and $[\varepsilon_{sf} \cdot d^2]$.

On the other hand the Effective Medium Approximation (EMA) contact model has also been employed to explain the permeability behaviour [34–36]. This model is based on the similitude between the Darcy's law and the equation to calculate the current flow in electricity. At certain porosity (a critical porosity, ε_c), a network of connected pores appears, resulting in a sudden increase in the permeability. At porosities around the critical porosity (which corresponds to the percolation threshold of porosity) the permeability (k) satisfies a scaling relation (Eq. 4):

$$k \propto (\varepsilon - \varepsilon_c)^t \quad \text{[Eq. 4]}$$

where t is the critical exponent.

Finally, the tortuosity factor of a membrane can be calculated using a simple model based on the Hagen-Poiseuille equation [Eq. 3] and the pore size distributions measured by mercury intrusion [37–39], as shown in Eq. 5.

$$\tau = \sqrt{\frac{\sum_{i=1}^{m}\left[\frac{a_i}{2}\left(r_{i_{max}}^4 - r_{i_{min}}^4\right) + \frac{b_i}{3}\left(r_{i_{max}}^3 - r_{i_{min}}^3\right)\right]}{8 \cdot \eta \cdot e^2 \cdot slp}} \quad \text{[Eq. 5]}$$

Where a_i and b_i are constants calculated from every interval i of the pore size distribution, r_{imax} and r_{imin} represent the maximum and minimum pore radius of every interval and slp the straight line's slope obtained in the water permeability test.

Although the research activity on low-cost microfiltration membranes has been very intense in the last years due to the many potential industrial applications of these materials very few papers have intended to model microstructural features of sintered membranes with functional properties of the membranes [40–42]. This is because the use of natural minerals (ball clays, kaolin, etc.) as raw materials makes it harder to model the intricate microstructure of these ceramic membranes.

As a consequence of the above, this research focuses on the relationship between microstructure and properties of low-cost ceramic microfiltration membranes. Hence, potato starch has been used as pore former and a mixture of kaolin and alumina as base composition. The objective was to determine the effect of starch addition at different weight percentages on the ceramic composition processing (by pressing) as well as on microstructure and permeation characteristics of the ceramic membranes. In addition, the effect of sintering temperature on the microstructure and performance of sintered membranes has been also addressed. Some equations have been assessed to model the permeability in function of structural parameters of the membranes.

2. Experimental

2.1. Membrane preparation

The raw materials used to prepare the ceramic membranes were alumina (AR12B5, Pechiney, France; D_{50}=5μm, S_e=12m^2/g) and kaolin (ER/N, Caobar, Spain; D_{50}=4.2μm). Potato starch (Sigma-Aldrich Co. USA; D_{50}=44.1 μm) was used as pore former. Table 1 shows the chemical composition of these materials.

Table 1. Chemical compositions of the raw materials used (wt%).

	Alumina	Kaolin
SiO_2	0.02	48.4
Al_2O_3	99.4	37.5
Fe_2O_3	0.01	0.53
CaO	0.01	0.10
Na_2O	0.37	-
K_2O	-	0.5
TiO_2	-	0.14
Loss on ignition	0.19	13.3

Seven compositions were formulated with different proportions of starch (0, 5, 10, 15, 20, 25, 30 wt %), maintaining a weight ratio 50:50 between alumina and kaolin (Table 2).

Table 2. Composition of the raw materials mixtures (wt%) used to prepare the membranes.

Ref	Alumina	Kaolin	Potato starch
S0	50	50	-
S5	47.5	47.5	5
S10	45	45	10
S15	42.5	42.5	15
S20	40	40	20
S25	37.5	37.5	25
S30	35	35	30

The raw materials were homogenised in acetone in a ball mill. The resulting suspension was dried under IR lamps and moistened to a content of 3 kg H_2O/100 kg dry solid, with an aqueous solution of 0.3 wt% polyvinyl alcohol (Mowiol 4-88, Clariant, Switzerland) which acted as binder. Cylindrical test specimens of 50 mm diameter and 6-7 mm thickness were formed by uniaxial dry pressing at 400 $kg \cdot cm^{-2}$ (Instron Model 6027, USA) and dried in an oven at 110ºC.

The green specimens were sintered in two steps, as shown in figure 1. Initially, the starch was oxidised in a muffle furnace with a slow firing cycle characterised by a maximum temperature of 500ºC (K60L, Nannetti Spa. Italy). Finally, the specimens were sintered in an electric kiln (RHF 1600, Carbolite, UK) with a thermal cycle characterised by a soaking time of 4 hours at maximum temperature (1100ºC or 1400ºC).

2.2. Membranes characterisation and equipment

The green and sintered bulk density of the specimens were determined by the Archimedes displacement technique using mercury as non-wetting liquid and the water uptake in sintered bodies was measured by the boiling water immersion method [43]. The permeability coefficient for water was obtained with a liquid permeameter (LEP101-A, PMI, USA). The pore size distribution of the membranes was measured by mercury intrusion porosimetry (AutoPore IV, Micromeritics Instruments Co, USA) and then the total volume of pores (V_f) and characteristic pore diameters (d_{16} and d_{50}) were calculated from experimental data. Additionally, the microstructure of some supports was analysed by scanning electron microscopy (FEG-ESEM Quanta 200 F, FEI, USA). Finally, the real density of the green and sintered samples was measured with a helium pycnometer (Utrapycnometer 1000, Quantachrome, USA).

3. Results and discussion

3.1. Bulk density and porosity of green membranes

As revealed by the figure 2 the bulk density of the green samples (BD_G) decreases when the starch content increases for two reasons: the real density of potato starch (1.51±0.02 g·cm^{-3}) is lower than that of the inorganic solid fraction (3.03±0.02 g·cm^{-3}) and a reduction of compaction during pressing occurs as a consequence of the ineffective plastic flow when starch is compressed. Nevertheless, there is an inflexion point at the starch content of 10 wt%, after which the slope decreases, showing a higher influence of the starch content on the bulk density of the green membranes. Green porosity (ε_G) slightly decreases with starch content following a quadratic function, since the introduction of starch causes the two-fold effect set out above for BD_G. The interaction of both effects produces the reduction of the green porosity

because porosity definition is based on the quotient between bulk and real density. Finally, the porosity that is theoretically obtained after discounting the volume occupied by starch (ε_{GT}) has been also calculated (Figure 2). When the volume occupied by starch is discounted (simulating the situation of the samples after the oxidation step during the thermal treatment), it is observed that green porosity without starch increases linearly with starch content confirming the negative contribution of starch to ceramic powder consolidation by pressing.

3.2. Microstructure assessment of sintered membranes

After sintering membranes without defects were obtained. These membranes presented enough strength so as to carry out characterisation tests. Figure 3 shows the crystalline phases of composition S0 sintered at both temperatures. The rest of sintered membranes which contained starch in the starting raw materials mixture displayed similar XRD patterns. Corundum and quartz appears at both temperatures, since they come respectively from alumina and kaolin, which contains a certain amount of quartz. At 1400ºC, mullite and cristobalite appears, because they are generated by the thermal treatment at temperatures higher than 1200ºC [42,44].

The bulk density of sintered membranes (BD_S) decreases linearly with starch content since the starch's combustion gives rise to pore volume formation (figure 4). Nevertheless, the bulk density also depends on the sintering temperature, augmenting when temperature changes from 1100ºC to 1400ºC, owing to a higher degree of sintering, as it can be seen in figure 4. As a consequence for any of the sintering temperatures tested, total porosity of sintered specimens (ε_S) increases linearly when starch content rises, since it is calculated on the basis of bulk density and average real density of the sintered composition (3.22±0.02 $g \cdot cm^{-3}$) (Figure 4). A similar tendency was also obtained by other authors using different starch contents and membrane's preparation methods [9,10,42,45].

In order to better follow the membrane densification process, a densification parameter (DP) was introduced as follows [46]:

$$DP = \frac{\varepsilon_{GT} - \varepsilon_S}{\varepsilon_{GT}} \quad \text{[Eq. 6]}$$

Where ε_S is the final porosity (for a given starch content and/or sintering temperature) and ε_{GT} is the initial porosity excluding starch.

DP shows the effects of the sintering temperature and starch content as plotted in figure 5. The value of densification parameter changes from negative to positive when temperature increases from 1100 ºC to 1400 ºC. In other words, it was observed that $\varepsilon_{GT}<\varepsilon_S$ for the lower temperature and $\varepsilon_{GT}>\varepsilon_S$ for the higher temperature. Considering that the linear shrinkage is very low at 1100 ºC, the negative densification parameters are probably the result of the loss of mass attributed to kaolin decomposition around 500 ºC as well as the predominance of surface transport mechanisms in the sintering process. By contrast, the positive densification parameters obtained at 1400 ºC relates to the advancement of sintering process, which probably takes place in presence of a liquid phase generated by the fluxing impurities present in the kaolin (see table 1). On the other hand, the effect of starch content is also dependent of sintering temperature. Thus at 1400ºC, densification parameter seems to slightly increase when starch content rises, but the total increment is lower than the experimental uncertainty. On contrary, at 1100ºC the densification parameter clearly decreases its absolute value as starch content augments due to the lower kaolin content in the composition and, in consequence, lower loss on ignition.

A deeper analysis on the development of membrane porosities was carried out on the basis of mercury pore sizing technique. Figure 6 displays the accumulate pore size distribution of membranes fired at the higher sintering temperature of 1400ºC. By introducing starch in the membrane's composition porosity increases and pore size distribution broadens as revealed by the marked arrow in the figure. These two parameters change at the same time as a consequence of the sintering process being impossible to alter one parameter without affecting the other one [42].

A better understanding of the types of porosity comprising the microstructure of the developed membranes can be found by plotting the corresponding differential pore size distribution curves. Figure 7 represents these curves for all the membranes sintered at 1100 ºC (a) and 1400 ºC (b). For the samples sintered at 1400 ºC the membrane without starch (S0) exhibits a bimodal distribution, as a result of its composition: small pores (around 0.1µm) mainly caused by the porosity of the matrix made up of the broken down kaolin particles and large pores (around 0.45µm), generated between the decomposed kaolin and alumina particles. The pore size grows (around 0.7µm) and the pore size distribution becomes wider

when reduced amounts of starch are added to the composition (less than 10 wt%). Nevertheless, the bimodal distribution becomes trimodal as well as the pore size dramatically increases when starch is added to the composition in high proportions (more than 10 wt%). This is because over this percentage of starch the large pores generated by starch burning out start to create a connected network accessible to the mercury introduced in the porosimetry measurement. The same trend has been found in the membranes sintered at 1100ºC (Figure 7a). The sintering temperature affects the porous structure in a different way as expected by the change in sintering mechanism as set out above. At 1400ºC a decreasing in the total pore volume and a coarsening of pores were detected as a consequence of the well reported Ostwald's Ripening effect [47,48].

The effect of the starch content on characteristics diameters (d_{16} and d_{50}) of membranes was also evaluated. As a consequence, a quadratic relation was observed between those parameters and starch content, whose polynomial coefficients were a function of the sintering temperature (Figure 8). This parabolic trend means that small differences in starch addition impact on membrane microstructure in a different way. Thus when higher starch proportions are used greater effect is observed. Largest pores (d_{16}) undergo higher influence of starch content because the starch employed in the research displayed a large particle size (D_{50}=44.1 μm) and, consequently, as recently reported, the generated pores associated to these particles burnout can reach up to 2-4 μm size [49,50]. Similar tendencies have been reported with membranes of different geometries prepared by other consolidation methods [9].

Figure 9 shows FEG-ESEM images of the extreme composition membranes (S0 and S30). As observed the microstructure of the membranes substantially changes when starch is added to the composition. Starch generates large and rounded pores in the ceramic matrix, composed of particles derived of kaolin and alumina (marked K and A respectively on the pictures) as extensively reported in similar low-cost ceramic membranes prepared with starch additions [9–11,50]. When sintering temperature increases from 1100ºC to 1400ºC, pores (marked P) become less rounded while areas of more sintered aspect develop. Although more rounded pores could be expected when sintering advances at higher temperature (1400ºC), the refractoriness of the alumina-kaolin matrix impedes this sintering effect. Cracks (marked C) around

large alumina particles are also observed as a consequence of the thermal stresses between alumina particles and kaolin-derived particles [51].

3.3. Water permeability

The permeability of the membranes in terms of water permeability coefficient (K_p) was determined using distilled water as a fluid. The relationship between K_p and starch addition has been represented in figure 10. As observed in this figure the amount of added starch drastically modifies the permeability coefficient, following an exponential trend at both sintering temperatures. These findings confirm the tendency reported in previous works [42]. However, despite the differences between the porosity (Figure 4) and pore sizes (Figure 8) of membranes sintered at 1100 and 1400ºC, the water permeability only displays a very slight dependence of sintering temperature, being higher at 1400ºC. These findings indicate that the contribution of the starch addition to membrane microstructure prevails on porosity differences (as shown in figure 4, which evidences that porosity of membranes sintered at 1400ºC is lower than that of the membranes sintered at 1100ºC). Hence, if we compare figures 8 and 10, water permeability variation with starch addition seems to follow the exponential change experienced by the coarse mean pore size (d_{16}) of the pore size distribution with the amount of starch; i.e. as coarse porosity is more and more present in the membrane (d_{16} increasing) water permeability grows. Moreover, the increase of coarse pore sizes with starch addition seems to be significant for starch addition higher than 10 wt%. This same finding was observed when the differential pore sizing analysis was presented (Figure 7). In that analysis, it was concluded that over 10 wt% starch addition the interconnection of the pore network created by the pore former starts to be effective. In other words, provided that a minimum amount of starch is added to the membrane composition (around 10 wt%) the starch content practically determines the value of water permeability of the ceramic membrane since the pores generated by the starch become interconnected and therefore accessible to fluids.

The open porosity (ε_W) has been calculated by means of water uptake and bulk density (Table 3) [50]. Applying the Hagen-Poiseuille equation [Eq 3] and assimilating ε_{sf} to ε_W, the relation between water permeability and the product [$\varepsilon_W \cdot d^2$] has been obtained at 1100 and 1400ºC, being d the characteristic pore diameters (d_{16}, d_{50}). Figure 11 shows that a linear trend is obtained for the two diameters, although

the correlation for d_{16} is slightly better as set out above on the contribution of coarse pores to water permeability.

Table 3. Open porosity (ε_W) of the membranes (%) calculated by means of water uptake and bulk density.

Ref	ε_W (%)
S0-1100	51.7
S10-1100	54.5
S20-1100	60.2
S30-1100	67.3
S0-1400	44.9
S5-1400	46.1
S10-1400	48.4
S15-1400	52.1
S20-1400	57.0
S25-1400	59.5
S30-1400	63.8

3.4. Percolation analysis

The relation between water permeability and open porosity (ε_W) has been evaluated by the EMA contact model for samples obtained at 1400ºC (Figure 12). For values of porosity lower than the critical porosity (percolation threshold of porosity), the water permeability varies linearly with open porosity. When porosity is higher than the critical porosity, the dependence follows the scaling relation [Eq. 4], where ε is porosity near porosity threshold (ε_c=51.64%) and obtained t value is 1.51. The calculated t is slightly higher than the reported value of approximately 1.2 given by other authors [34–36]. Nevertheless, the critical porosity calculated corresponds to a starch content of 10.2 wt% which agrees quite well with the estimates deduced along the previous experimental representations. To sum up, the dependence of water permeability at 1400ºC with open porosity presents two trenches:

$\varepsilon < \varepsilon_c \rightarrow a + b \cdot \varepsilon$

$\varepsilon \geq \varepsilon_c \rightarrow a + b \cdot \varepsilon + c \cdot (\varepsilon - \varepsilon_c)^t$

being a, b and c constants values (see figure 12). Although this relationship could not be calculated at 1100ºC because of the reduced number of samples available, the similar shape of both curves predicts that it should follow the same model.

3.5. Tortuosity estimation

Physically, tortuosity factor (τ) is defined as the ratio of the actual distance Δl travelled by the permeating species per unit length Δx of the filtrating medium [52]. There are no experimental methods to directly evaluate the tortuosity and, in consequence, it is usually estimated by theoretical equations or empiric models [52]. In this section the tortuosity factor is estimated by a simple model [eq. 5] based on the Hagen-Poiseuille equation [eq. 3] and the pore size distributions determined by mercury intrusion. This model has been successfully used in previous research with other low-cost ceramic membrane compositions [37–39]. The data have been collected from the previous sections and plotted in figure 7. Overall the higher the starch content or the sintering temperature the lower the tortuosity factor is. This matches well with microstructure observations by FEG-ESEM (Figure 6) as well as with the findings set out on pore sizing curves and water permeability. Hence, when temperature rises from 1100 to 1400ºC, despite the observed porosity reduction the effect of sintering diminishes tortuosity by pore coarsening effect leading to water permeability increasing. Starch added to the composition develops a connected coarse pores network, which also reduces the tortuosity of the pore channels giving rise to an effective water permeability increase. Nevertheless, samples obtained with 15 wt% starch addition do not match the others (tortuosity factor is 17) and have not been included in the figure 13. This unexpected lack of correlation is probably related to the fact that those membranes were obtained separately (in a different experimental test) from the rest of the samples; therefore it can be deduced that the composition preparation process strongly influences the tortuosity value (considered as a parameter related with the local microstructure) but it does not show any effect on the rest of variables (water permeability and pore size distribution parameters, considered as global parameters).

4. Conclusions

In this investigation, potato starch has been employed as a pore former for preparing low-cost ceramic membranes by uniaxial dry-pressing. The starting composition was based on the alumina-kaolin system and different starch percentages were added to the same. Two sintering temperatures (1100 ºC and 1400 ºC) were tested.

It was observed that the different weight percentage of potato starch did affect the properties of the membrane. Thus porosity of sintered membranes linearly increased with starch content since the starch's combustion gave rise to pores. The porosity also depends on the sintering temperature, decreasing when temperature changes from 1100ºC to 1400ºC, owing to a higher degree of sintering, as a consequence of a change in the sintering mechanism. On the other hand, pore size distribution also changes with starch addition. In particular coarse pore size fraction strongly increases when starch is added to the composition in higher proportions (more than 10 wt%) owing to the development of a connected pore network. Permeability tests confirm that the starch content practically determines the value of water permeability of the ceramic membrane since the pores generated by the starch become interconnected and therefore accessible to fluids. Experimental data of water permeability fit the the Hagen-Poiseuille equation confirming the significant contribution of coarse pores generated by starch to membrane permeability.

A percolation analysis evaluated by the EMA contact model allowed to conclude that the critical porosity calculated corresponds to a starch content of 10.2 wt% which agrees quite well with the estimates deduced from microstructure inspection and pore size determination by mercury porosimetry. Finally, the tortuosity factor was estimated by a simple model based on the Hagen-Poiseuille equation and the pore size distributions. The estimates showed that tortuosity factor decreased as the starch content or sintering temperature increased. These findings again confirm that starch added to the composition develops a connected coarse pores network which also reduces the tortuosity of the pore channels giving rise to an effective membrane permeability increase.

Acknowledgements

The authors thank Spanish Ministerio de Economía y Competitividad their support for the development of this research (Plan Nacional de I+D, ref. CTQ2012-37450-C02-02).

References

[1] M. Mulder, Basic Principes of Membrane Technology, 2nd ed., Kluwer Academic Publishers, Dordrecht, The Netherlands, 1996.

[2] A.J. Burggraf, L. Cot, eds., Fundamentals of Inorganic Membranes, Science and Technology, Elsevier, Amsterdam, 1996.

[3] N. Saffaj, M. Persin, S.A. Younsi, A. Albizane, M. Cretin, A. Larbot, Elaboration and characterization of microfiltration and ultrafiltration membranes deposited on raw support prepared from natural Moroccan clay: Application to filtration of solution containing dyes and salts, Appl. Clay Sci. 31 (2006) 110–119. http://dx.doi.org/10.1016/j.clay.2005.07.002.

[4] S. Khemakhem, A. Larbot, R. Ben Amar, New ceramic microfiltration membranes from Tunisian natural materials: Application for the cuttlefish effluents treatment, Ceram. Int. 35 (2009) 55–61. http://dx.doi.org/10.1016/j.ceramint.2007.09.117.

[5] S. Fakhfakh, S. Baklouti, Elaboration and characterisation of low cost ceramic support membrane, Adv. Appl. Ceram. 109 (2010) 31–38. http://dx.doi.org/10.1179/174367609X422234.

[6] S. Khemakhem, A. Larbot, R. Ben Amar, Study of performances of ceramic microfiltration membrane from Tunisian clay applied to cuttlefish effluents treatment, Desalination. 200 (2006) 307–309. http://dx.doi.org/10.1016/j.desal.2006.03.327.

[7] A. Lhassani, J. Bentama, Modeling of mass transfer sintered clay membranes for application to treat water, Desalination. 179 (2005) 335–338. http://dx.doi.org/10.1016/j.desal.2004.11.079.

[8] N. Saffaj, S.A. Younsi, M. Persin, M. Cretin, A. Albizane, A. Larbot, Processing and characterization of $TiO_2/ZnAl_2O_4$ ultrafiltration membranes deposited on tubular support prepared

from Moroccan clay, Ceram. Int. 31 (2005) 205–210. http://dx.doi.org/10.1016/j.ceramint.2004.05.001.

[9] G.C.C. Yang, C.-M. Tsai, Effects of starch addition on characteristics of tubular porous ceramic membrane substrates, Desalination. 233 (2008) 129–136. http://dx.doi.org/10.1016/j.desal.2007.09.035.

[10] M.M. Bazin, M.A. Ahmat, N. Zaidan, A.F. Ismail, N. Ahmad, Effect of starch addition on microstructure and strength of ball clay membrane, J. Teknol. (Sciences Eng. 69 (2014) 117–120.

[11] F. Bouzerara, A. Harabi, S. Condom, Porous ceramic membranes prepared from kaolin, Desalin. Water Treat. 12 (2009) 415–419. http://dx.doi.org/10.5004/dwt.2009.1051.

[12] A. Harabi, F. Zenikheri, B. Boudaira, F. Bouzerara, A. Guechi, L. Foughali, A new and economic approach to fabricate resistant porous membrane supports using kaolin and $CaCO_3$, J. Eur. Ceram. Soc. 34 (2014) 1329–1340. http://dx.doi.org/10.1016/j.jeurceramsoc.2013.11.007.

[13] A. Harabi, A. Guechi, S. Condom, Production of supports and filtration membranes from Algerian kaolin and limestone, Procedia Eng. 33 (2012) 220–224. http://dx.doi.org/10.1016/j.proeng.2012.01.1197.

[14] M.R. Weir, E. Rutinduka, C. Detellier, Fabrication, characterization and preliminary testing of all-inorganic ultrafiltration membranes composed entirely of a naturally occurring sepiolite clay mineral, J. Memb. Sci. 182 (2001) 41–50.

[15] S. Masmoudi, A. Larbot, H. El Feki, R. Ben Amar, Elaboration and properties of new ceramic microfiltration membranes from natural and synthesised apatite, Desalination. 190 (2006) 89–103. http://dx.doi.org/10.1016/j.desal.2005.03.097.

[16] S. Masmoudi, A. Larbot, H. El Feki, R. Ben Amar, Elaboration and characterisation of apatite based mineral supports for microfiltration and ultrafiltration membranes, Ceram. Int. 33 (2007) 337–344. http://dx.doi.org/10.1016/j.ceramint.2005.10.001.

[17] A. Majouli, S.A. Younssi, S. Tahiri, A. Albizane, H. Loukili, M. Belhaj, Characterization of flat membrane support elaborated from local Moroccan perlite, Desalination. 277 (2011) 61–66. http://dx.doi.org/10.1016/j.desal.2011.04.003.

[18] A. Majouli, S. Tahiri, S. Alami Younssi, H. Loukili, A. Albizane, Elaboration of new tubular ceramic membrane from local Moroccan perlite for microfiltration process. Application to treatment of industrial wastewaters, Ceram. Int. 38 (2012) 4295–4303. http://dx.doi.org/10.1016/j.ceramint.2012.02.010.

[19] I. Barrouk, S. Alami Younssi, A. Kabbabi, A. Albizane, M. Raquif, J. Maghnouj, et al., Preparazione di supporti ceramici a base di fosfato naturale del Marocco per l'elaborazione di membrane di microfiltrazione e ultrafiltrazione, Ceram. Spec. 3 (2009) 177–186.

[20] I. Barrouk, S. Alami Younssi, A. Kabbabi, M. Persin, A. Albizane, S. Tahiri, New ceramic membranes from natural Moroccan phosphate for microfiltration application, Desalin. Water Treat. (2014) 1–8. http://dx.doi.org/10.1080/19443994.2014.915386.

[21] J.-H. Eom, Y.-W. Kim, S.-H. Yun, I.H. Song, Low-cost clay-based membranes for oily wastewater treatment, J. Ceram. Soc. Japan. 122 (2014) 788–794. http://dx.doi.org/10.2109/jcersj2.122.788.

[22] J. Zhou, X. Zhang, Y. Wang, A. Larbot, X. Hu, Elaboration and characterization of tubular macroporous ceramic support for membranes from kaolin and dolomite, J. Porous Mater. 17 (2010) 1–9. http://dx.doi.org/10.1007/s10934-008-9258-z.

[23] D. Vasanth, G. Pugazhenthi, R. Uppaluri, Fabrication and properties of low cost ceramic microfiltration membranes for separation of oil and bacteria from its solution, J. Memb. Sci. 379 (2011) 154–163. http://dx.doi.org/10.1016/j.memsci.2011.05.050.

[24] B.K. Nandi, R. Uppaluri, M.K. Purkait, Preparation and characterization of low cost ceramic membranes for micro-filtration applications, Appl. Clay Sci. 42 (2008) 102–110. http://dx.doi.org/10.1016/j.clay.2007.12.001.

[25] D. Vasanth, G. Pugazhenthi, R. Uppaluri, Cross-flow microfiltration of oil-in-water emulsions using low cost ceramic membranes, Desalination. 320 (2013) 86–95. http://dx.doi.org/10.1016/j.desal.2013.04.018.

[26] L. Palacio, Y. Bouzerdi, M. Ouammou, A. Albizane, J. Bennazha, A. Hernandez, et al., Ceramic membranes from Moroccan natural clay and phosphate for industrial water treatment, Desalination. 245 (2009) 501–507. http://dx.doi.org/10.1016/j.desal.2009.02.014.

[27] I. Jedidi, S. Khemakhem, L. Messouadi, A. Larbot, M. Rafiq, L. Cot, et al., Elaboration and characterisation of fly ash based mineral supports for microfiltration and ultrafiltration membranes, Ceram. Int. 35 (2009) 2747–2753. http://dx.doi.org/10.1016/j.ceramint.2009.03.021.

[28] E. Chevalier, D. Chulia, C. Pouget, M. Viana, Fabrication of porous substrates: a review of processes using pore forming agents in the biomaterial field, J. Pharm. Sci. 97 (2008) 1135–1154.

[29] N. Ahmad, N. Zaidan, Effect of sintering temperature on membrane properties of Sayong ball clay, Appl. Mech. Mater. 315 (2013) 349–353. http://dx.doi.org/10.4028/www.scientific.net/AMM.315.349.

[30] D. Vasanth, R. Uppaluri, G. Pugazhenthi, Influence of sintering temperature on the properties of porous ceramic support prepared by uniaxial dry compaction method using low-cost raw materials for membrane applications, Sep. Sci. Technol. 46 (2011) 1241–1249. http://dx.doi.org/10.1080/01496395.2011.556097.

[31] P. Monash, G. Pugazhenthi, Development of ceramic supports derived from low-cost raw materials for membrane applications and its optimization based on sintering temperature, Int. J. Appl. Ceram. Technol. 8 (2011) 227–238. http://dx.doi.org/10.1111/j.1744-7402.2009.02443.x.

[32] P. Maarten Biesheuvel, H. Verweij, Design of ceramic membrane supports: permeability, tensile strength and stress, J. Memb. Sci. 156 (1999) 141–152. http://dx.doi.org/10.1016/S0376-7388(98)00335-4.

[33] M.J. Matteson, C. Orr, Filtration. Principles and Practices., 2nd ed., Marcel Dekker, INC., New York, 1987.

[34] A. Mikrajuddin, F.G. Shi, S. Chungpaiboonpatana, K. Okuyama, C. Davidson, J.M. Adams, Onset of electrical conduction in isotropic conductive adhesives: a general theory, Mater. Sci. Semicond. Process. 2 (1999) 309–319. http://dx.doi.org/10.1016/S1369-8001(99)00035-9.

[35] A. Mikrajuddin, Khairurrijal, Gelation Model for Porosity Dependent Fluid Permeability in Porous Materials, J. Mat. Dan. Sains. 14 (2009) 15–19.

[36] Masturi, Silvia, M.P. Aji, E. Sustini, Khairurrijal, M. Abdullah, Permeability, strength and filtration performance for uncoated and titania-coated clay wastewater filters, Am. J. Environ. Sci. 8 (2012) 79–94. http://www.scopus.com/inward/record.url?eid=2-s2.0-84859132292&partnerID=tZOtx3y1.

[37] S. Sales, Intercambiadores iónicos inorgánicos nanoestructurados: síntesis e infiltración en membranas cerámicas. PhD thesis, Universitat Jaume I, 2015.

[38] J. Gilabert, Relación del coeficiente de permeabilidad de membranas cerámicas con las condiciones de síntesis. MsC thesis, Universitat Jaume I, 2012.

[39] M.-M. Lorente-Ayza, S. Mestre, M. Menéndez, E. Sánchez, Comparison of extruded and pressed low cost ceramic microfiltration membranes, J. Eur. Ceram. Soc. (2015) in press. http://dx.doi.org/ 10.1016/j.jeurceramsoc.2015.06.010.

[40] W. Li, W. Xing, N. Xu, Modeling of relationship between water permeability and microstructure parameters of ceramic membranes, Desalination. 192 (2006) 340–345. http://dx.doi.org/10.1016/j.desal.2005.07.042.

[41] J. Marchese, M. Almandoz, M. Amaral, L. Palacio, J.I. Calvo, P. Pradanos, et al., Fabricación y caracterización de membranas cerámicas tubulares para microfiltración, Bol. Soc. Esp. Ceram. V. 39 (2000) 215–219.

[42] E. Sánchez, S. Mestre, V. Pérez-Herranz, M. García-Gabaldón, Síntesis de membranas cerámicas para la regeneración de baños de cromado agotados, Bol. Soc. Esp. Ceram. V. 44 (2005) 409–414.

[43] A. Barba, V. Beltrán, C. Feliu, J. García-Ten, F. Ginés, E. Sánchez, et al., Materias primas para la fabricación de soportes de baldosas cerámicas, 2nd ed., Instituto de Tecnología Cerámica, Castellón, 2000.

[44] E. Sánchez, S. Mestre, V. Pérez-Herranz, M. García-Gabaldón, Ceramic membranes for continuous regeneration of spent chromium plating baths, Key Eng. Mater. 264-268 (2004) 2211–2214.

[45] F.A. Almeida, E.C. Botelho, F.C.L. Melo, T.M.B. Campos, G.P. Thim, Influence of cassava starch content and sintering temperature on the alumina consolidation technique, J. Eur. Ceram. Soc. 29 (2009) 1587–1594. http://dx.doi.org/10.1016/j.jeurceramsoc.2008.10.006.

[46] R.M. German, Sintering, theory and practice, John Wiley & Sons, New York, 1996.

[47] S.J. Kang, Sintering. Densification, grain growth & microstructure, Elsevier Ltd, Oxford, 2005.

[48] M. Rahaman, Ceramic processing and sintering, 2nd ed., Marcel Dekker, INC., New York, 2003.

[49] S. Sales, M.-M. Lorente-Ayza, J. Gilabert Albiol, E. Sánchez, S. Mestre, Efecto de las características del almidón sobre la permeabilidad de las membranas cerámicas, in: XIII Congr. Nac. Mater., Barcelona, 2014: p. 115.

[50] M.-M. Lorente-Ayza, M.J. Orts, V. Pérez-Herranz, S. Mestre, Role of starch characteristics in the properties of low-cost ceramic membranes, J. Eur. Ceram. Soc. 35 (2015) 2333–2341. http://dx.doi.org/10.1016/j.jeurceramsoc.2015.02.026.

[51] F.A. Gilabert, V. Cantavella, M. Dal Bó, E. Sánchez, Modeling microstructural damage of silicate-based ceramics and its influence on macroscopic fracture strength, Acta Mater. 70 (2014) 30–44. http://dx.doi.org/10.1016/j.actamat.2014.01.026.

[52] L. Shen, Z. Chen, Critical review of the impact of tortuosity on diffusion, Chem. Eng. Sci. 62 (2007) 3748–3755. http://dx.doi.org/10.1016/j.ces.2007.03.041.

Glossary

K_P: specific permeability to water (m^2)

ε_{sf}: surface porosity

ε_C: critical porosity

ε_G: green porosity

ε_{GT}: porosity theoretically obtained after discounting the volume occupied by starch

ε_S: sintered total porosity

ε_W : open porosities calculated by means of water absorption and bulk density

τ: tortuosity factor

BD_G: bulk density of the green samples

BD_S: bulk density of sintered membranes

DP: densification parameter

Figure captions

Figure 1. Thermal cycles for the two temperatures used to sinter the membranes.

Figure 2. Bulk density (BD_G) and porosity (ε_G) of green membranes of the different compositions; calculated porosity excluding the starch is also showed (ε_{GT}).

Figure 3. Diffractogram of membrane S0 at 1100 and 1400ºC.

Figure 4. Influence of the starch content on the bulk density (BD_S) and total porosity (ε_S) of sintered membranes.

Figure 5. Relation between the densification parameter (DP) and the starch content of the membrane composition.

Figure 6. Accumulate pore size distributions of the membranes sintered at 1400ºC.

Figure 7. Differential pore size distributions of the membranes sintered at a) 1100ºC and b)1400ºC.

Figure 8. Influence of starch content on characteristics diameters d_{16} and d_{50} of the sintered membranes.

Figure 9. SEM micrographs of the membranes S0 at 1100ºC and 1400ºC and S30 at 1100ºC and 1400ºC.

Figure 10. Influence of starch content on water permeability coefficient (K_P)

Figure 11. Relation between the water permeability and the coefficient ($\varepsilon_W \cdot d^2$), being d the characteristic pore diameters (d_{16} and d_{50}).

Figure 12. Relation between open porosity calculated by means of water absorption and bulk density (ε_W) and water permeability and model to evaluate percolation threshold of porosity.

Figure 13. Relation between tortuosity factor (τ) and starch content of the membrane composition, following the model set out in [37–39].

Tables

Table 1. Chemical compositions of the raw materials used (wt%).

Table 2. Composition of the raw materials mixtures (wt%) used to prepare the membranes.

Table 3. Open porosity (ε_W) of the membranes (%) calculated by means of water uptake and bulk density.

Table 1. Chemical compositions of the raw materials used (wt%).

	Alumina	Kaolin
SiO_2	0.02	48.4
Al_2O_3	99.4	37.5
Fe_2O_3	0.01	0.53
CaO	0.01	0.10
Na_2O	0.37	-
K_2O	-	0.5
TiO_2	-	0.14
Loss on ignition	0.19	13.3

Table 2. Composition of the raw materials mixtures (wt%) used to prepare the membranes.

Ref	Alumina	Kaolin	Potato starch
S0	50	50	-
S5	47.5	47.5	5
S10	45	45	10
S15	42.5	42.5	15
S20	40	40	20
S25	37.5	37.5	25
S30	35	35	30

Table 3. Open porosity (ε_W) of the membranes (%) calculated by means of water uptake and bulk density.

Ref	ε_W (%)
S0-1100	51.7
S10-1100	54.5
S20-1100	60.2
S30-1100	67.3
S0-1400	44.9
S5-1400	46.1
S10-1400	48.4
S15-1400	52.1
S20-1400	57.0
S25-1400	59.5
S30-1400	63.8

Figure 1
Click here to download high resolution image

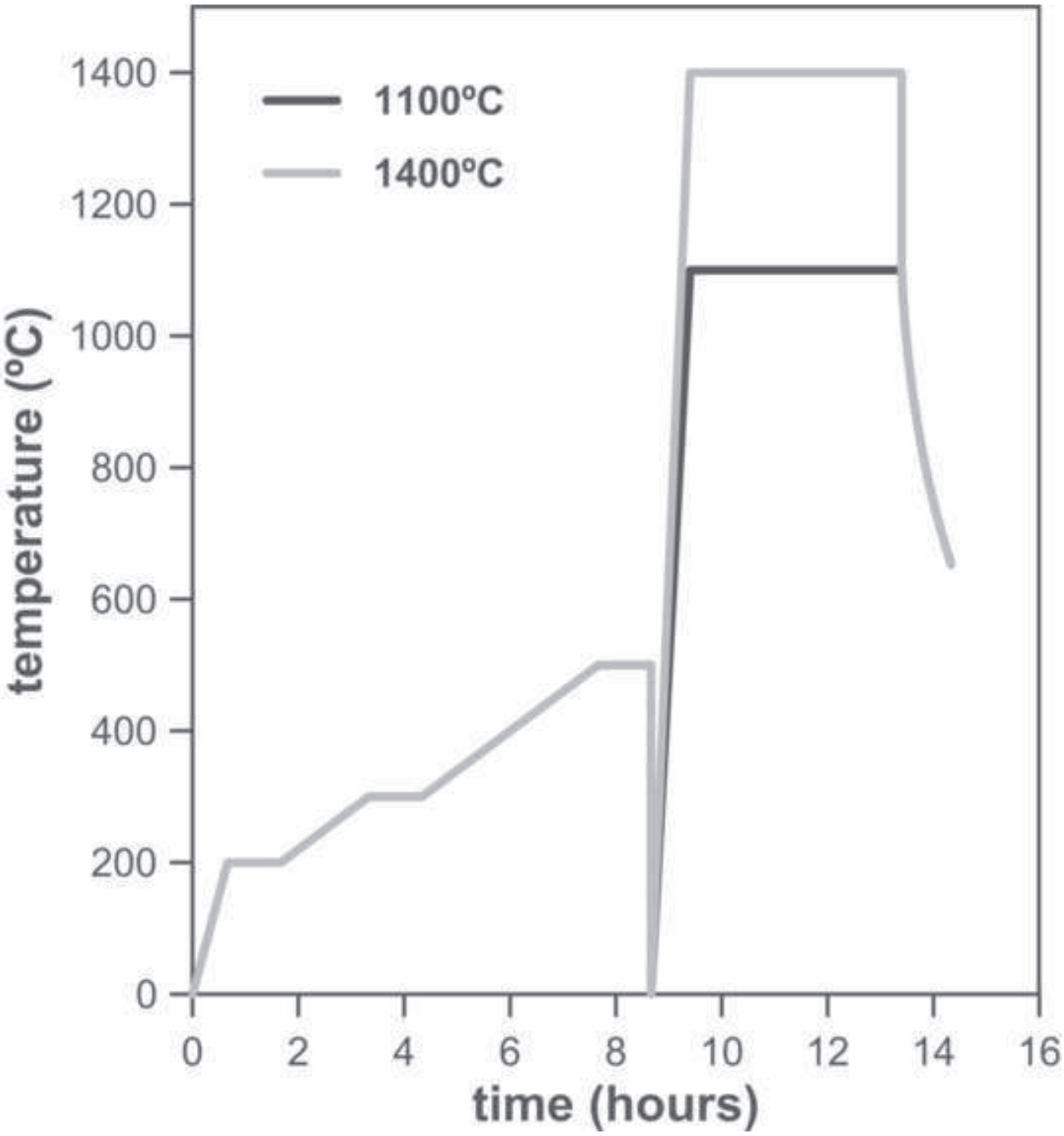

Figure 2
Click here to download high resolution image

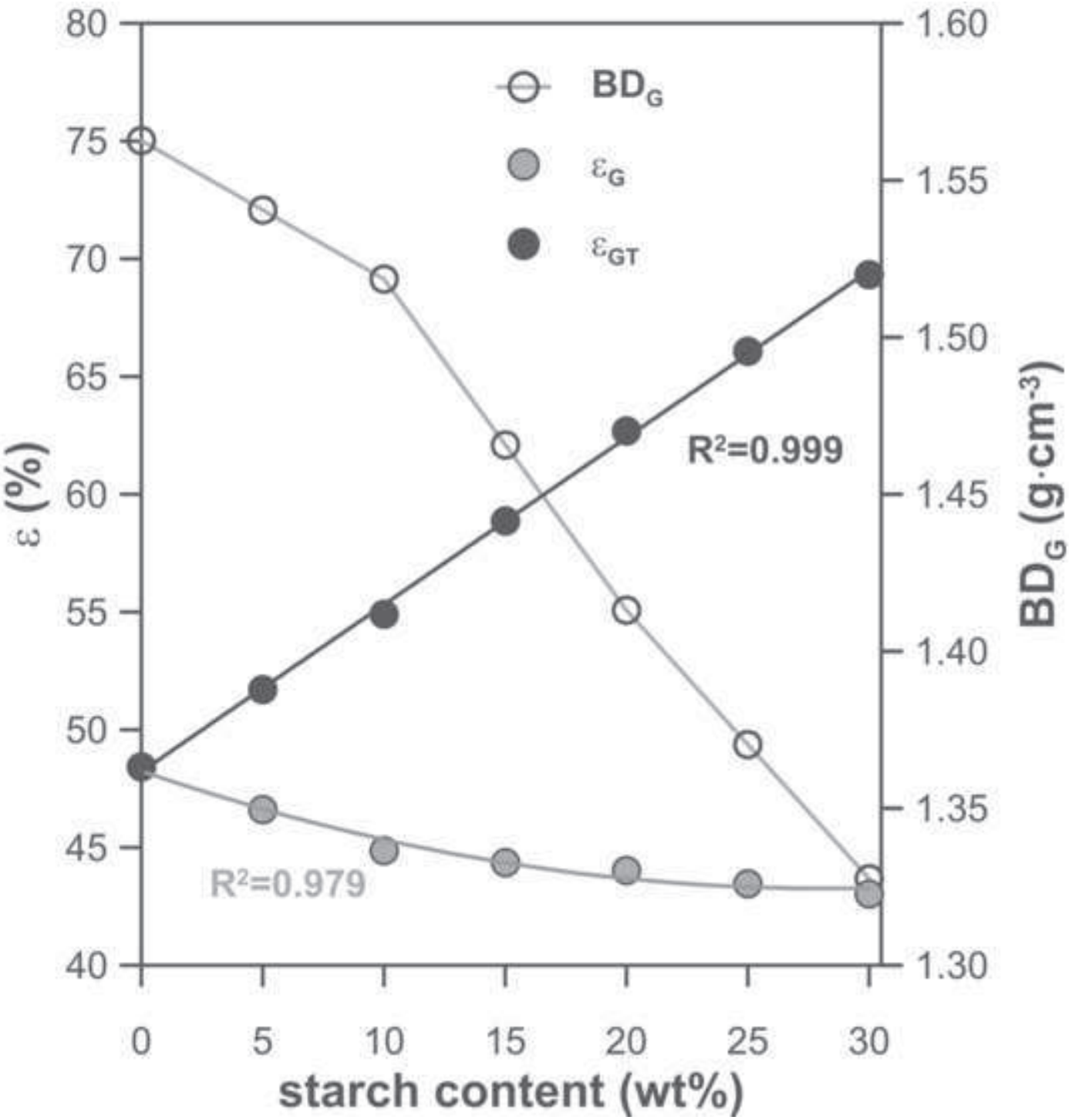

Figure 3
Click here to download high resolution image

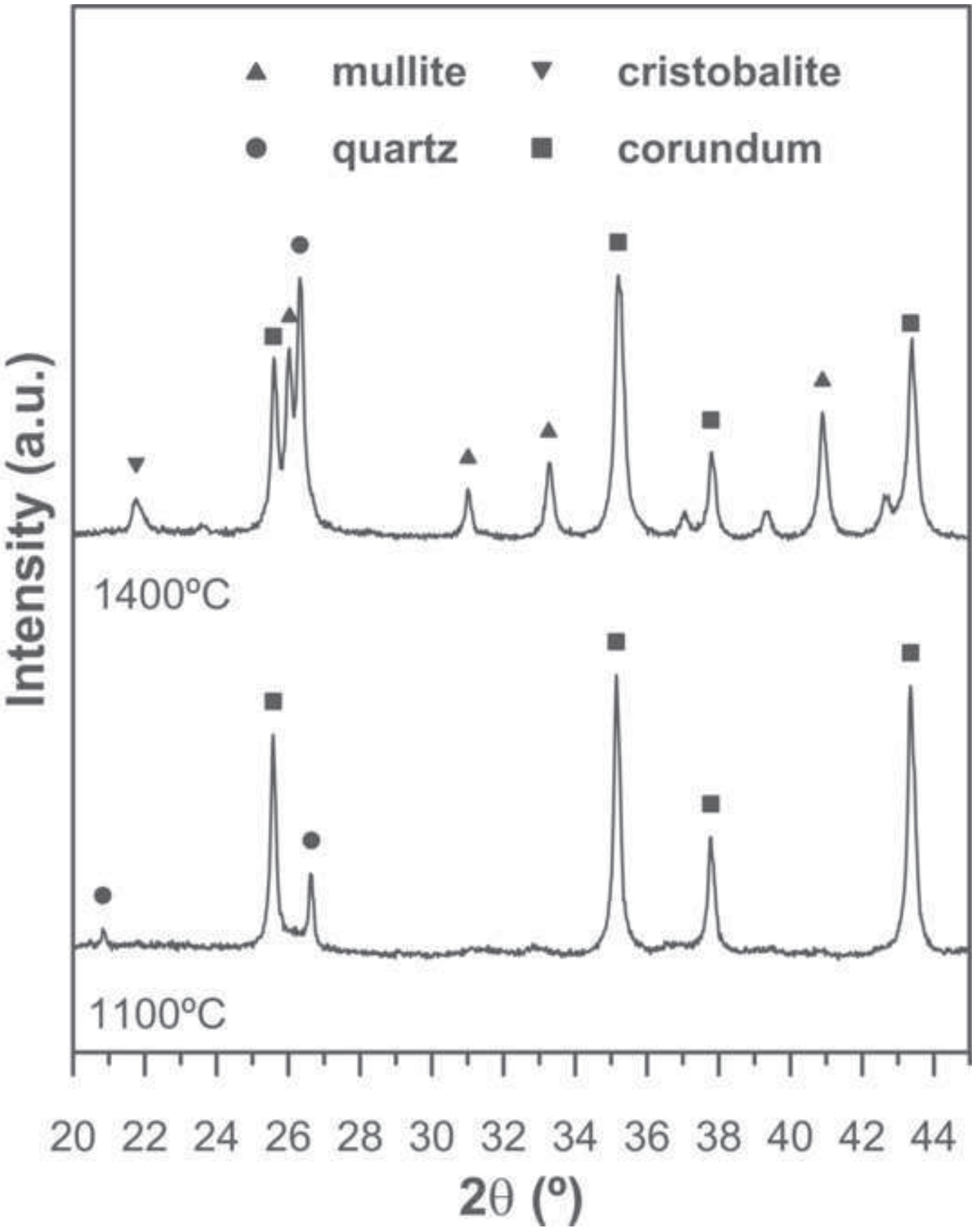

Figure 4
Click here to download high resolution image

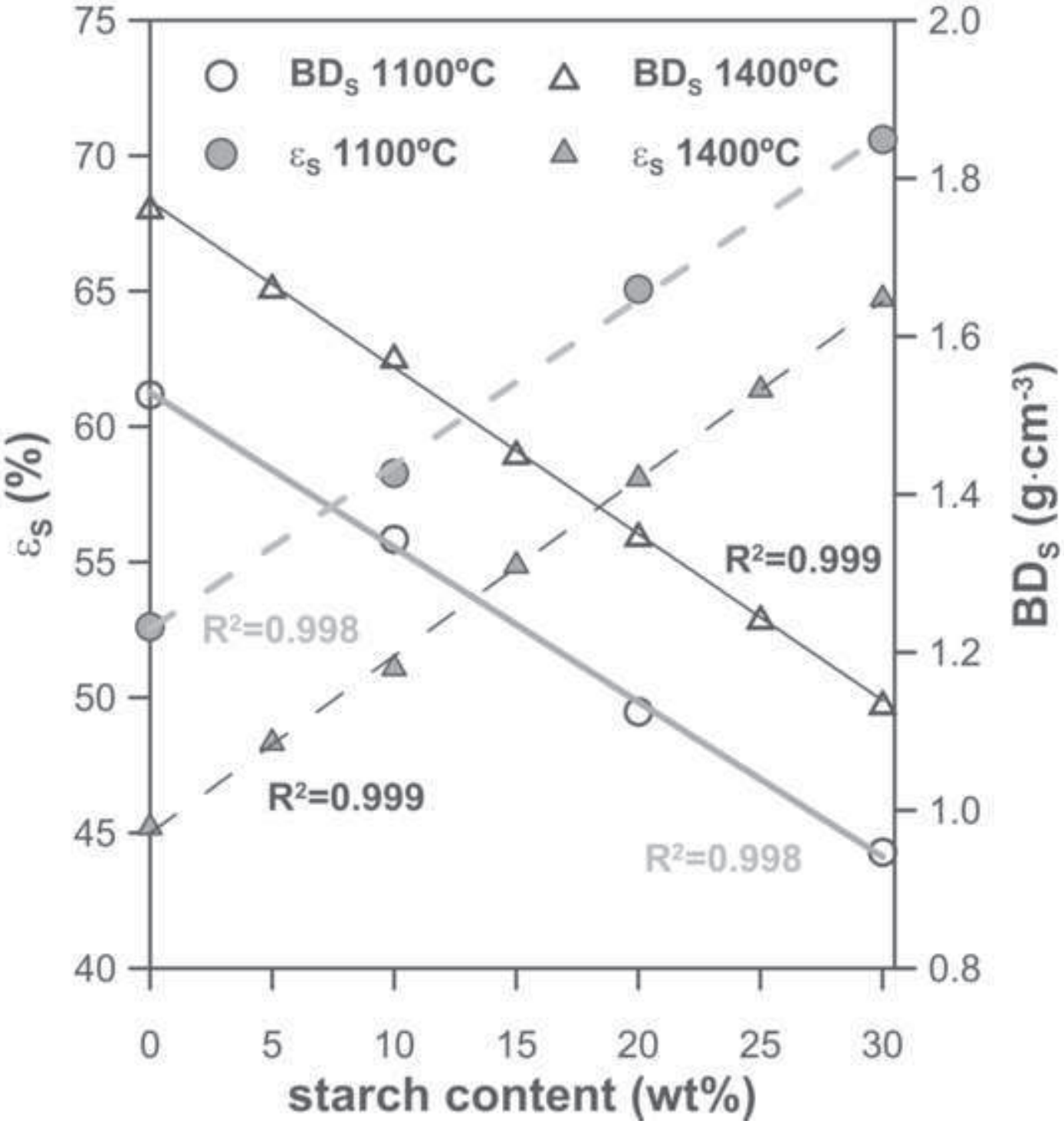

Figure 5
Click here to download high resolution image

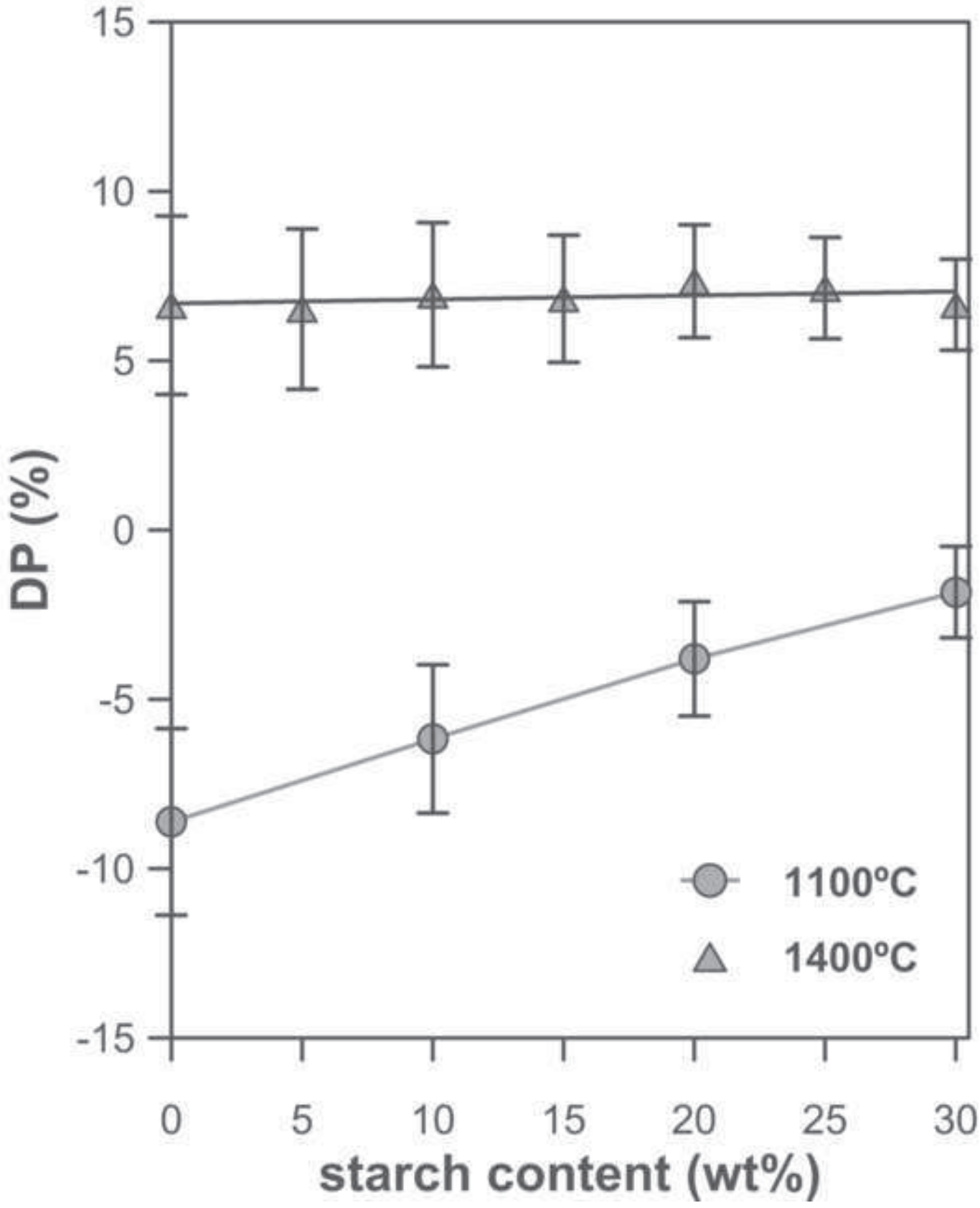

Figure 6
Click here to download high resolution image

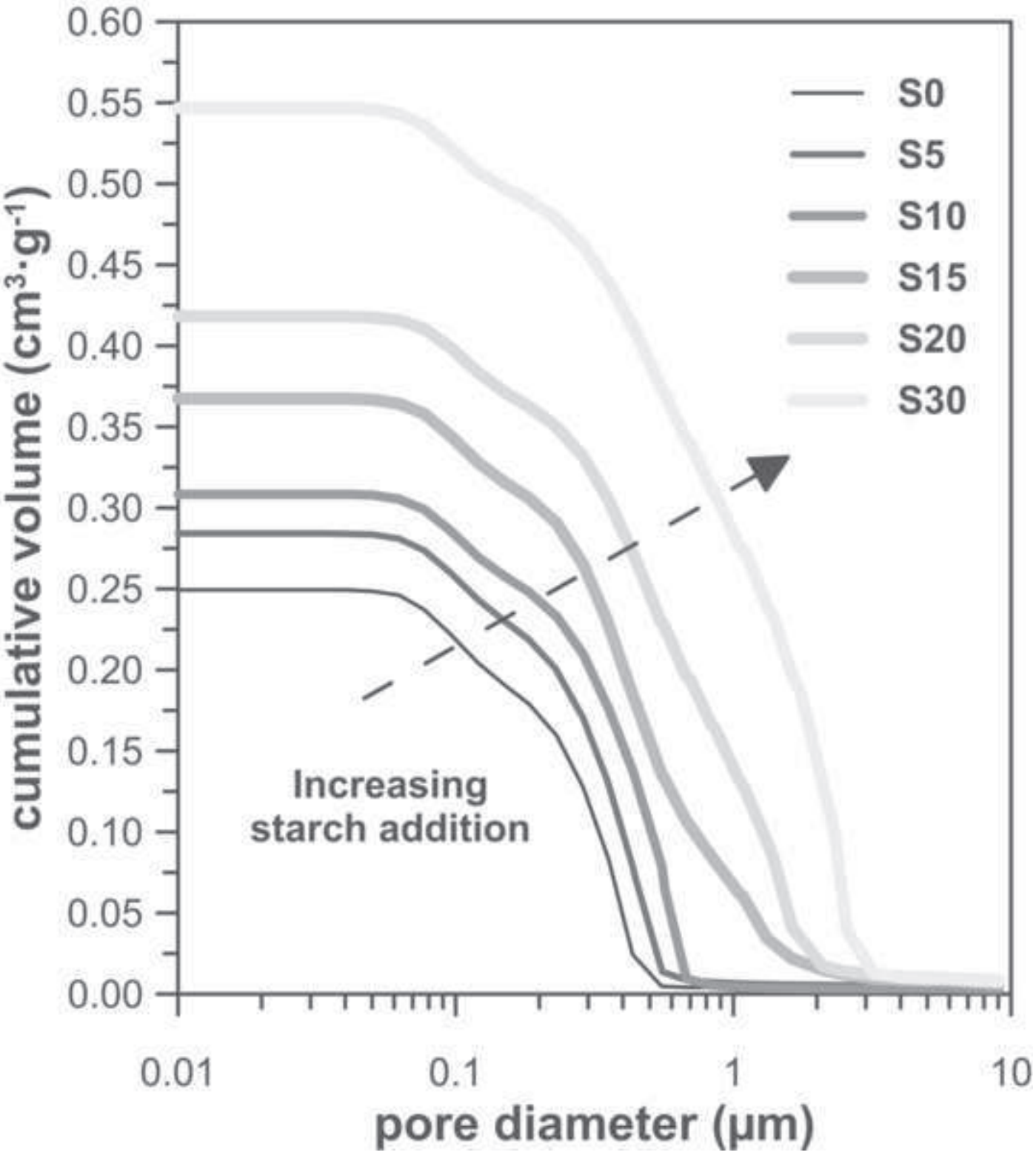

Figure 7
Click here to download high resolution image

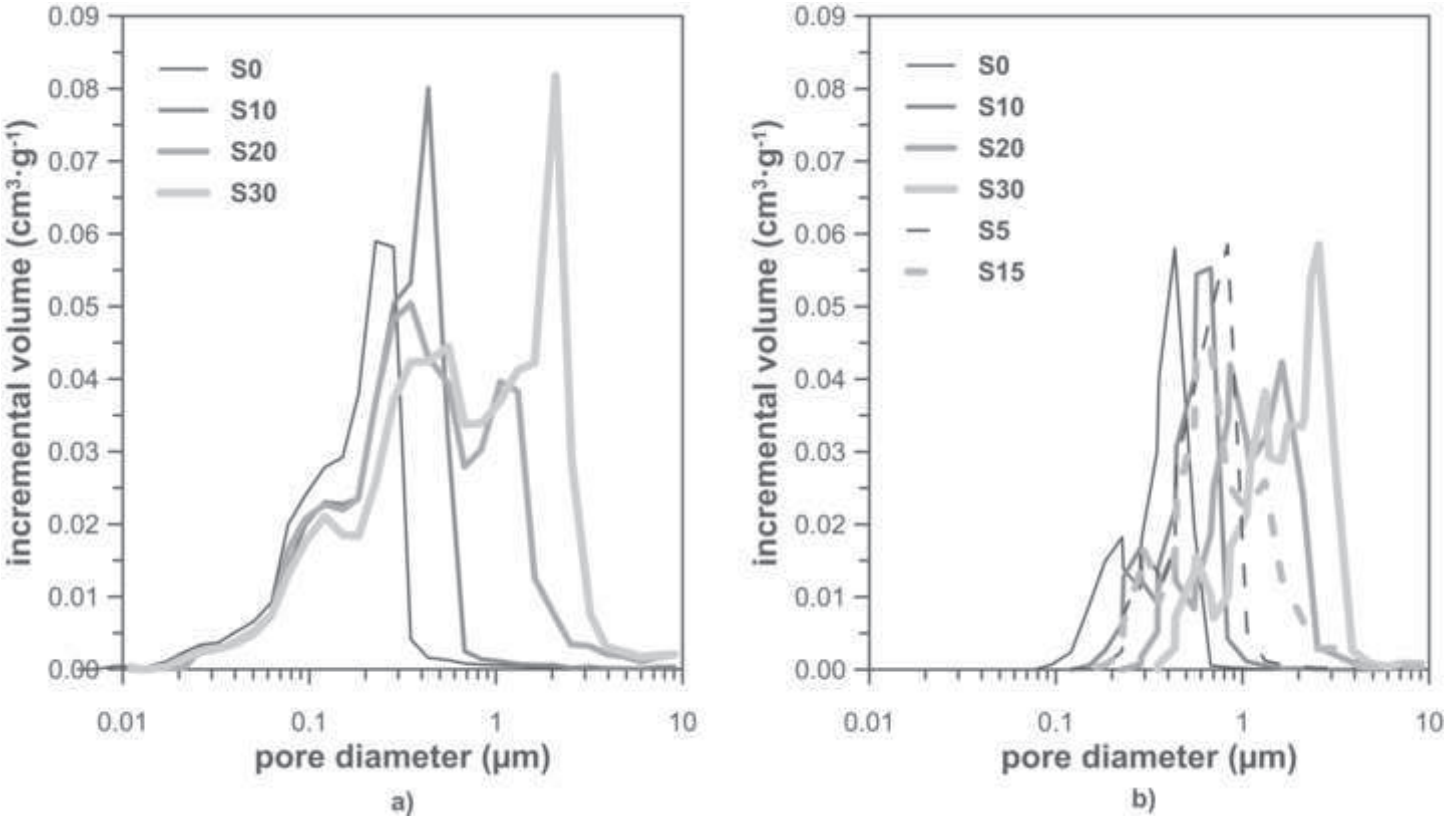

Figure 8
Click here to download high resolution image

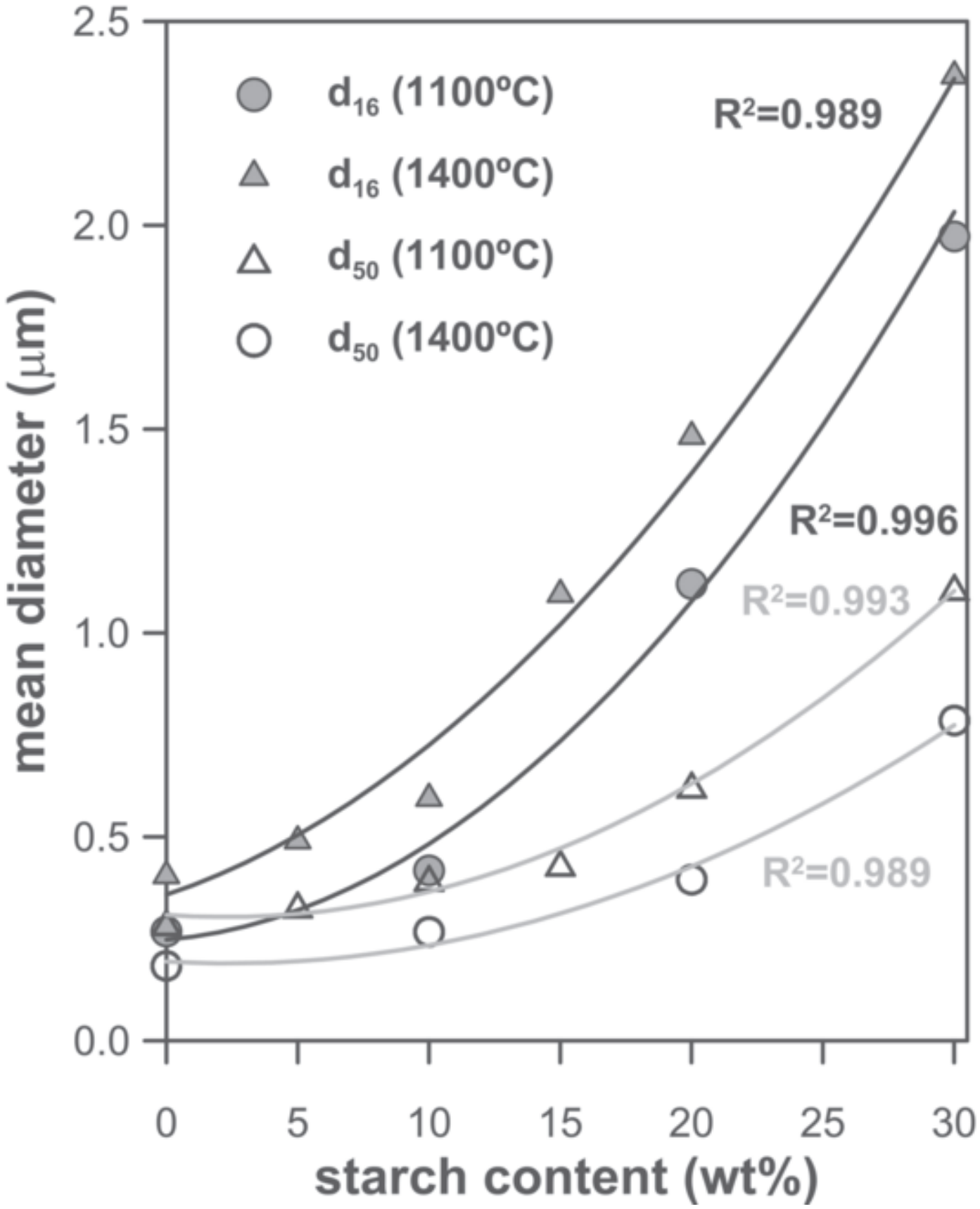

Figure 9
Click here to download high resolution image

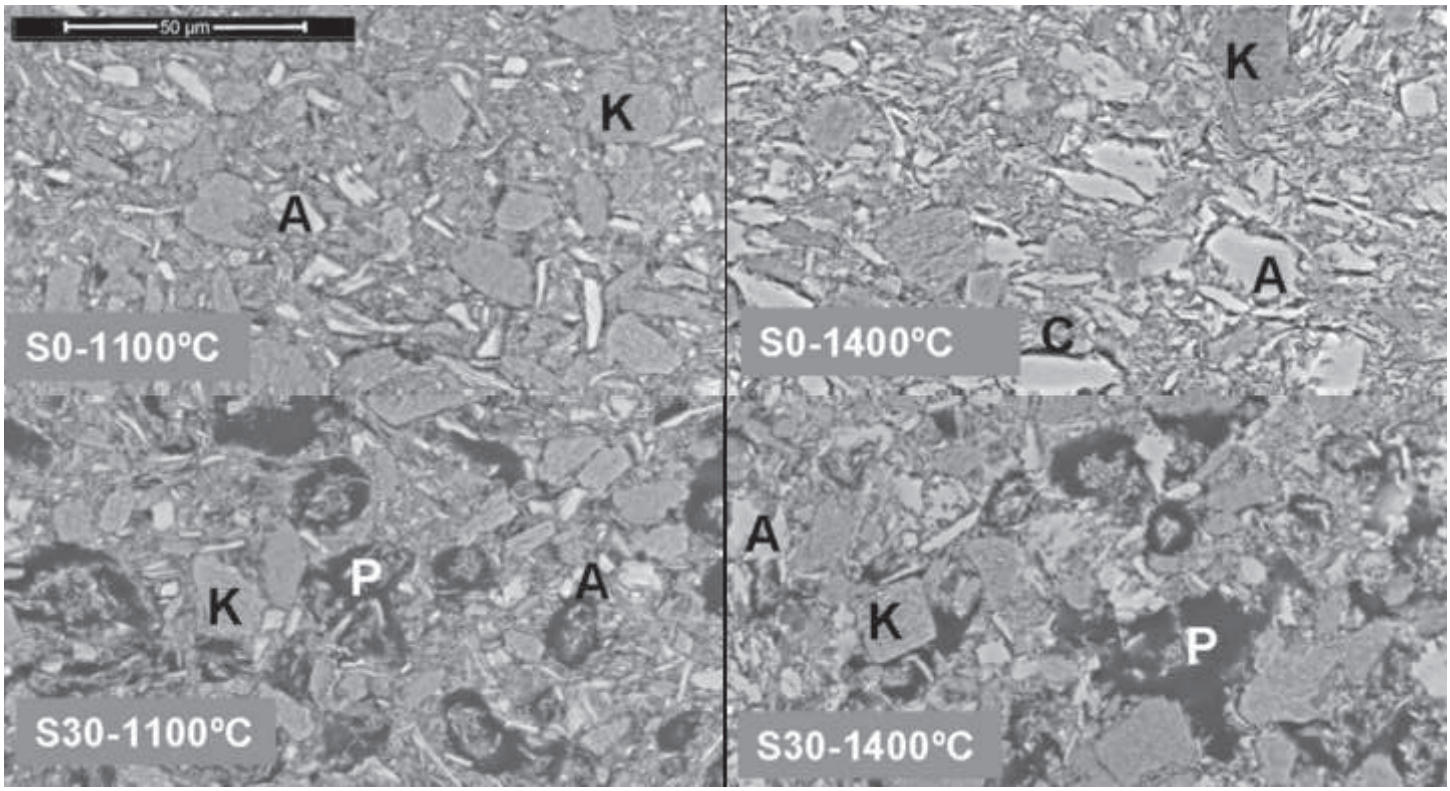

Figure 10
Click here to download high resolution image

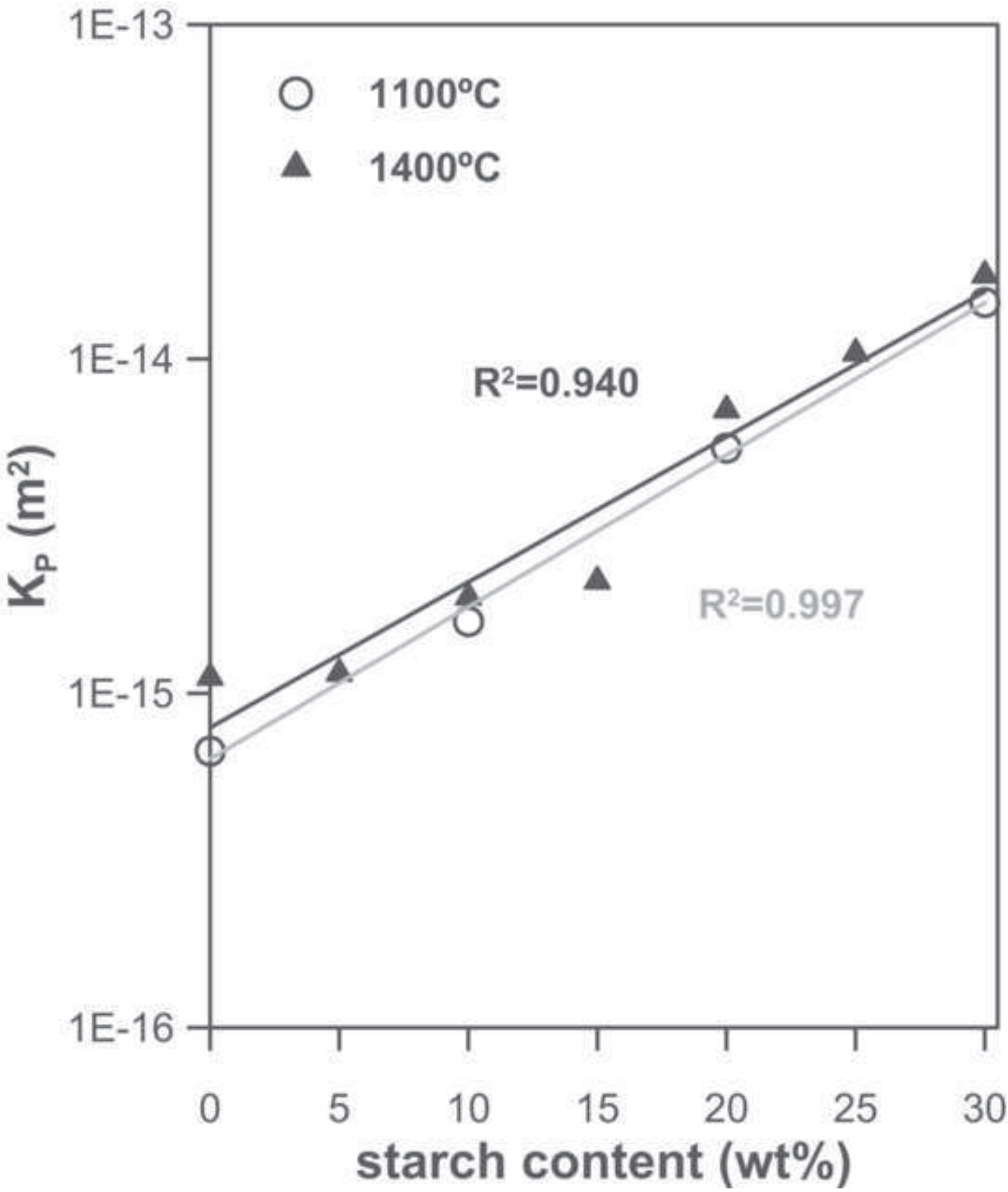

Figure 11
Click here to download high resolution image

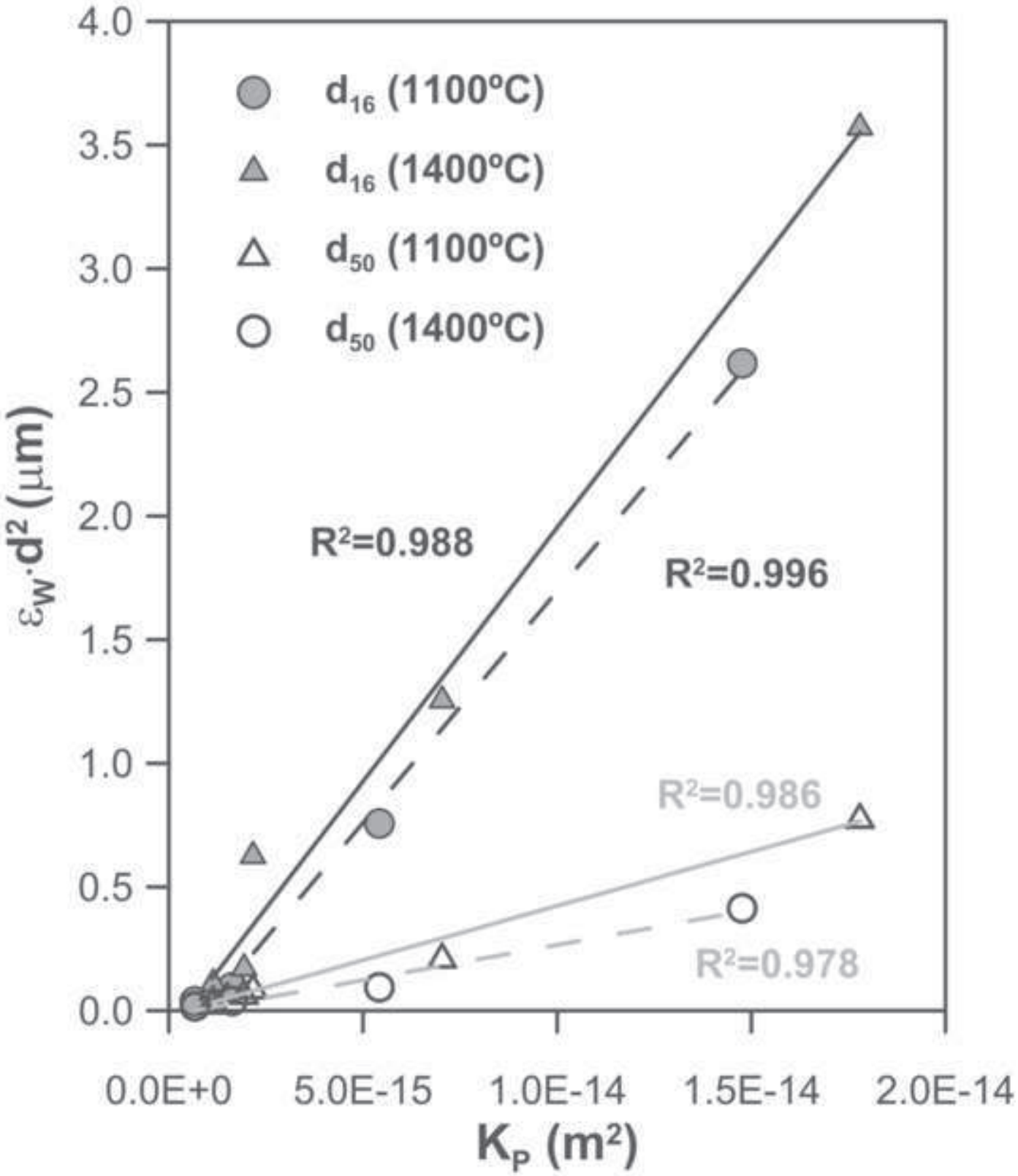

Figure 12
Click here to download high resolution image

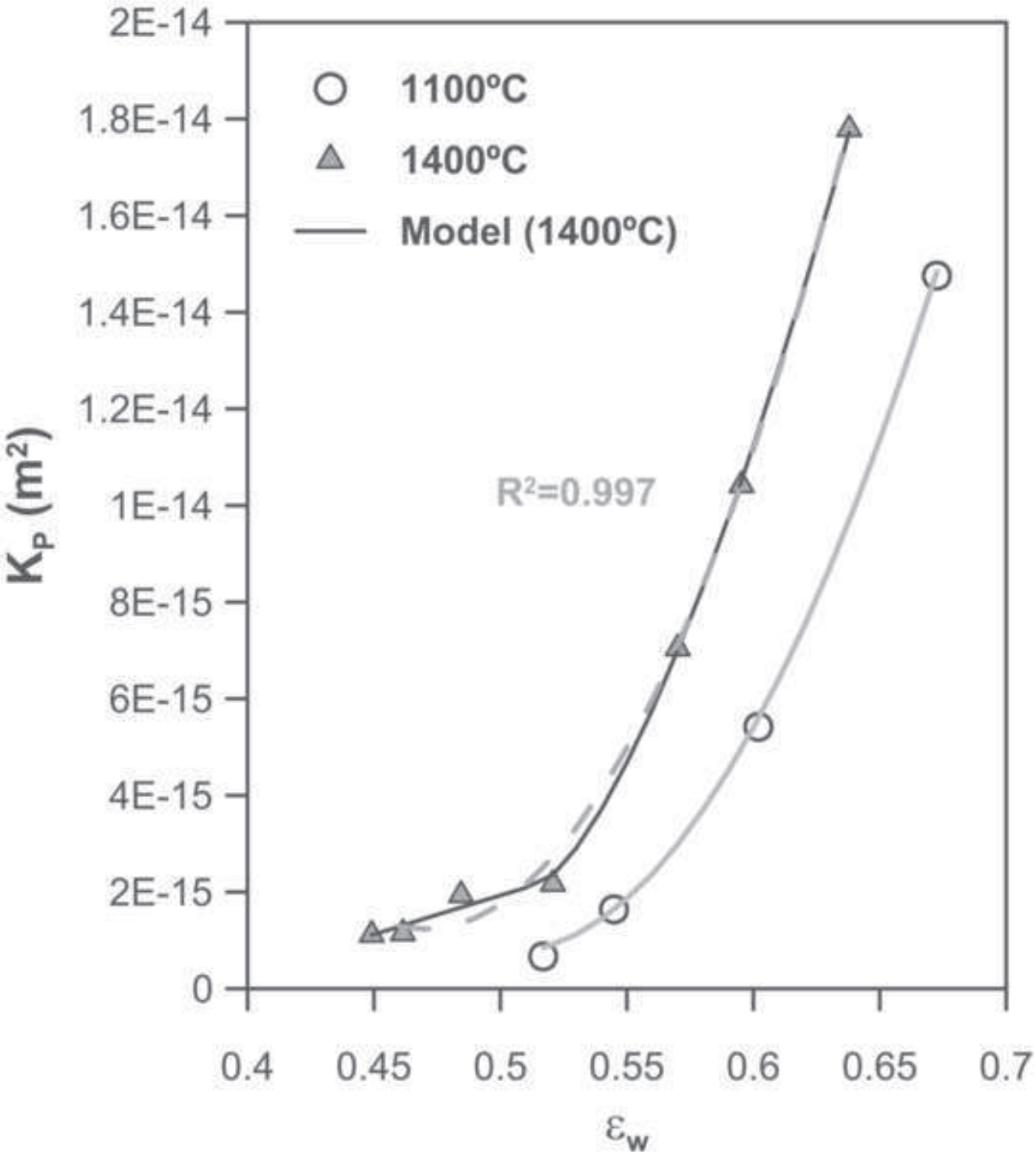

Figure 13
Click here to download high resolution image